

Weak action potential backpropagation is associated with high-frequency axonal firing capability in principal neurons of the gerbil medial superior olive

Luisa L. Scott, Travis A. Hage and Nace L. Golding

Section of Neurobiology and Institute for Neuroscience, University of Texas at Austin, Austin, TX 78712-0248, USA

Principal neurons of the medial superior olive (MSO) convey azimuthal sound localization cues through modulation of their rate of action potential firing. Previous intracellular studies *in vitro* have shown that action potentials appear highly attenuated at the soma of MSO neurons, potentially reflecting specialized action potential initiation and/or a physically distant site of generation. To examine this more directly, we made dual patch-clamp recordings from MSO principal neurons in gerbil brainstem slices. Using somatic and dendritic whole-cell recordings, we show that graded action potentials at the soma are highly sensitive to the rate of rise of excitation and undergo strong attenuation in their backpropagation into the dendrites (length constant, 76 μm), particularly during strong dendritic excitation. Using paired somatic whole-cell and axonal loose-patch recordings, we show that action potentials recorded in the axon at distances $> 25 \mu\text{m}$ are all-or-none, and uniform in amplitude even when action potentials appear graded at the soma. This proximal zone corresponded to the start of myelination in the axon, as assessed with immunocytochemical staining for myelin basic protein in single-labelled neurons. Finally, the axon was capable of sustaining remarkably high firing rates, with perfect entrainment occurring at frequencies of up to 1 kHz. Together, our findings show that action potential signalling in MSO principal neurons is highly secure, but shows a restricted invasion of the somatodendritic compartment of the cell. This restriction may be important for minimizing distortions in synaptic integration during the high frequencies of synaptic input encountered in the MSO.

(Received 12 May 2007; accepted after revision 9 July 2007; first published online 12 July 2007)

Corresponding author Nace L. Golding: Section of Neurobiology, C0920, University of Texas at Austin, Austin, TX 78712-0248, USA. Email: golding@mail.utexas.edu

The medial superior olive (MSO) is a constituent nucleus of the brainstem circuitry for processing sound localization cues. MSO principal neurons compute the horizontal location of low-frequency sounds using the differences in the time required for sounds to propagate to each ear. These interaural time delays (ITDs) are submillisecond cues whose physiological range is dependent upon the diameter of the animal's head. To extract these brief ITDs, principal neurons of the MSO detect convergence in the timing of binaural excitatory inputs segregated onto each limb of the bipolar dendritic trees of the neurons (Lindsey, 1975). The integration of these excitatory inputs, which are phase-locked to frequencies up to 2 kHz, is further influenced by phase-locked inhibition restricted to the soma (Kapfer *et al.* 2002; Brand *et al.* 2002). Although modulation of firing rate with changing ITDs is a defining feature of neurons in the MSO (Goldberg & Brown, 1969; Yin & Chan, 1990; Spitzer & Semple, 1995; Brand

et al. 2002), the underlying cellular mechanisms are still uncertain (for reviews see Grothe, 2003; Palmer, 2004; Joris & Yin, 2007).

Modelling studies have highlighted the fact that the sensitivity of binaural integration in ITD-coding neurons is highly sensitive to the spatial relationships between the excitatory and inhibitory inputs and the axon (Agmon-Snir *et al.* 1998; Zhou *et al.* 2005). Recent findings in birds have shown that the physical location and length of the spike-generating region within the axon is an important determinant of the sensitivity of the cell to high-frequency synaptic inputs (Kuba *et al.* 2006). Many details concerning action potential generation have yet to be determined in mammalian ITD-coding neurons. Our previous findings have shown that the axon emanates from the soma or proximal dendrite of MSO principal neurons (Scott *et al.* 2005; Smith, 1995), and that action potentials are initiated at an unspecified location within the axon

(Scott *et al.* 2005). Once initiated, action potentials propagate back into the soma and the dendrites. The small and variable action potentials that appear at the soma of MSO neurons (Scott *et al.* 2005) could arise from distal initiation and corresponding attenuation of the backpropagating signal, as proposed by Yin & Chan (1990). However, proximal initiation with marked but variable attenuation of the signal, or the initiation of graded action potentials in the axon itself, also remain as possibilities. The extent to which action potentials continue to propagate into the dendrites has yet to be fully characterized. Important not only to binaural integration, the temporal coincidence between backpropagating action potentials and synaptic excitation in the dendrites has been proposed as a developmental mechanism for the refinement of ITD sensitivity (Gerstner *et al.* 1996).

Although the properties of action potential signalling are central to the encoding of binaural information, there have been no studies to systematically address the initiation and propagation of action potentials in MSO principal neurons. Based on studies combining loose-patch and whole-cell recordings, it is apparent that axonal signalling capabilities differ according to neuron type. In cerebellar and hippocampal neurons, spike frequency at which action potentials fail to propagate effectively in the axon varies considerably, although generally small somatic spikes do not propagate well (Khaliq & Raman, 2005; Meeks *et al.* 2005; Monsivais *et al.* 2005). There is also considerable evidence for heterogeneity in the efficacy of action potential backpropagation into the dendrites. This heterogeneity is based on differences in both dendritic morphology and ion channel expression (Stuart *et al.* 1997; Häusser *et al.* 2000).

In the current study, we have used paired simultaneous recordings from the soma and axon to examine action potential initiation and propagation in MSO principal neurons. Our results are consistent with a proximal axonal site of action potential initiation and all-or-none signalling in the axon despite strong and variable attenuation of action potentials in the soma. The fidelity of axonal transmission was extraordinarily high, with single axons capable of transmitting trains of brief depolarizations of the soma at frequencies up to 1000 Hz. Thus, action potential initiation and propagation in MSO principal neurons is specialized to provide faithful high-frequency transmission in the axon while perhaps minimizing disruption of synaptic integration in the soma.

Methods

Ethical approval

All experimental procedures were approved by the Institutional Animal Care and Use Committee at the University of Texas at Austin in accordance with the

United States Animal Welfare Act and the US Public Health Services' Policy on the Humane Use and Care of Laboratory Animals.

Slice preparation

A total of 154 Mongolian gerbils (*Meriones unguiculatus*) were obtained from Charles River Laboratories (Wilmington, MA, USA) or bred at the Animal Resource Center of the University of Texas at Austin. Gerbils are an apt model system for this study because, unlike other small rodents, they have a low-frequency hearing range overlapping largely with that of humans and a well-developed MSO. Dendritic and axonal recordings were restricted to gerbils between postnatal day (P) 14 and 19, within the first week after onset of hearing (~P12). Axonal recordings at older ages were technically difficult, as the heavier myelination obscured adequate visualization of the small-diameter axonal processes using conventional epifluorescence optics. At P14–19, although the electrophysiological properties of MSO principal neurons undergo age-dependent changes (Scott *et al.* 2005), their characteristic features of small, graded action potentials and fast membrane time constants have been established.

Gerbils were anaesthetized via the inhalation of halothane. After the cessation of the eye-blink reflex, animals were decapitated and the brain was removed while submerged in artificial cerebrospinal fluid (ACSF) containing (in mM): NaCl 125, KCl 2.5, CaCl₂ 2, MgSO₄ 1, NaHCO₃ 25, NaH₂PO₄ 1.25 and glucose 25, pH adjusted to 7.45 with NaOH, and saturated with 95% O₂–5% CO₂. Coronal sections (200 μm) were cut at 32°C using an oscillating tissue slicer (Leica VT-1000S, Solms, Germany) and then transferred to an incubating chamber containing oxygenated ACSF at 35°C. After 30 min, slices were held at room temperature (22–25°C) until recording. Individual slices were transferred to a recording stage and bathed with oxygenated ACSF maintained at 35°C during recording.

Whole-cell recording

MSO neurons were visualized using infrared differential interference contrast microscopy (Zeiss Axioskop 2FS Plus, Oberkochen, Germany) in combination with a newvicon tube camera (Dage-MTI, Michigan City, IN, USA). Somatic recordings were made using heat-polished borosilicate patch pipettes (o.d., 1.65 mm; World Precision Instruments, Sarasota, FL, USA) with open tip resistances of 2–4 MΩ (somatic electrodes) and 6–11 MΩ (dendritic electrodes). The internal solution in whole-cell patch pipettes contained (in mM): potassium gluconate 115, KCl 20, sodium phosphocreatine 10, EGTA 0.5, MgATP 4, NaGTP 0.3 and HEPES 10; pH adjusted to

7.3 with KOH. Biocytin (0.1%) was also included in the internal solution for subsequent morphological analyses of the recorded cells. Somatic and dendritic recordings were made with Dagan BVC-700A amplifiers in current-clamp mode (Minneapolis, MN, USA) using bridge balance and capacitance compensation. Activation of synaptic inputs to MSO cells was achieved by delivering brief (100 μ s) electrical pulses to the slice through patch pipettes broken to tip diameters of ~ 10 μ m. Pulses were generated by a constant current stimulator (Digitimer, Hertfordshire, UK). Stimulation electrodes were placed medial or lateral to the MSO. Somatically injected current steps or simulated excitatory postsynaptic currents (EPSCs; bi-exponential waveform, 0.2 ms rise and 0.2 ms decay; 3.5 ms duration) also were used to evoke responses. The identification of recorded cells was made on the basis of their location in the slice, cell body shape, and responses to depolarizing current steps. Additionally, most cells were successfully labelled with biocytin and their morphology was examined after recordings (see below). Recordings were included if the series resistance was < 15 M Ω at the soma and < 50 M Ω for dendritic recordings. Data were low-pass filtered at 5 kHz and acquired at 50–100 kHz using custom-made macros programmed in IgorPro (WaveMetrics, Inc., Lake Oswego, OR, USA).

Loose-patch recording

For dual somatic and axonal recordings, 30 μ M Alexa 488 in the internal solution allowed visualization of the axon using epifluorescence imaging in conjunction with a cooled CCD camera (Photometrics Cascade 512B, Tuscon, AZ, USA). Five to 15 min after patching the soma, a second patch pipette (3–4 M Ω) filled with 145 mM NaCl, 10 mM HEPES and < 10 μ M Alexa 488 (pH 7.45) was guided to the axon and negative pressure was applied to pull a short length of axon into the lumen of the pipette (70–90 M Ω). Once this loose patch configuration was achieved, pressure was typically released during the recording. Loose-patch recordings were made with Dagan BVC-700A amplifiers in current-clamp mode without bridge balance or capacitance compensation. All loose-patch recordings included in this study had action potential signals that were at least 3.5 standard deviations above the noise floor. Recordings were restricted to those > 25 μ m from the soma, because in more proximal recordings a negative wave preceded and summated with the positive wave (Meeks *et al.* 2005). A similar phenomenon was found during a few of the dual somatic whole-cell and loose-patch recordings used to test the sensitivity of the recording technique. For the dual somatic recordings, this preceding negative wave or 'sink' was considered to be an artifact of the geometric relationship between the two recording pipettes and the axon, and

these recordings were not used. Data were low-pass filtered at 1–3 kHz and acquired at 100 kHz using custom-made macros programmed in IgorPro.

Anatomy

Slices with biocytin-labelled cells were fixed in 4% paraformaldehyde and subsequently processed using an avidin-biotin horse radish peroxidase reaction (ABC Kit, nickel-enhanced 3, 3'-diaminobenzidine as a chromagen, Vectorlabs, Burlingame, CA, USA). MSO principal neurons were verified by their location in the slice, and by cell morphology. Cells were traced at 40 \times using an Axioskop FS2 with a camera lucida. Axonal recording location was also measured at 40 \times using a Zeiss Axiocam CCD camera (Thornwood, NY, USA) and Openlab 3.1.4 Software (Improvision, Lexington, MA, USA). Recording sites were usually apparent by a small loop of axon and/or could be cross-checked with the epifluorescent images taken during the recording. To determine the relative tonotopic location of individual neurons, slices with biocytin-filled cells were imaged under a dissecting microscope (Leica MZFIII) at 10 \times using oblique light to visualize the dorsal and ventral boundaries of the MSO. Under these lighting conditions, the nucleus was darker than the surrounding areas (see Fig. 2A). The dorsal-ventral axis was divided into thirds and cell location was determined by which third contained the centre of the soma (measurements made in OpenLab 3.1.4).

Dual-label immunohistochemistry

Coronal slices were prepared as above. Brief whole-cell current-clamp recordings confirmed that cells had transient responses. Slices with biocytin-labelled cells were fixed in 4% paraformaldehyde, washed in PBS, incubated in blocking buffer (10% normal goat serum, 0.5% Triton X-100 and 1% DMSO) for 1 h, and moved to blocking buffer with 1:1000 Texas Red-conjugated streptavidin (Molecular Probes, Carlsbad, CA, USA) for 2 h. Slices were washed in PBS, submerged in 20% sucrose, embedded in gelatin, and cut at 20 μ m on a freezing-sliding microtome. Thin sections were then placed in DMSO for 15 min, washed in PBS, incubated in blocking buffer (10% normal goat serum, 0.5% Triton X-100 and 1% DMSO) for at least 1 h, and moved to blocking buffer with 1:100 sheep anti-myelin basic protein (Chemicon, Temecula, CA, USA) for 2 days. Sections were washed 6 \times 10 min in PBS, incubated in secondary antibody buffer (blocking buffer with 1:1000 Alexa-488-conjugated donkey anti-sheep) for 2 h, washed in PBS and mounted on slides coverslipped with Mowiol 4-88 mounting medium (Calbiochem, San Diego, CA, USA). Neurons were imaged with a confocal microscope (Leica SP2 AOBs).

Analysis

All electrophysiological analyses were completed in IgorPro. Somatic action potential amplitude was measured from the inflection point. Rise times for the underlying excitatory postsynaptic potential (EPSP) were measured between the start of the EPSP to the action potential inflection point. At least 20 synaptically evoked action potentials were analysed for each cell. Relative refractory period and entrainment were determined from the response at the axonal recording site during trains of somatically injected stimuli. Relative refractory period was determined by the probability of the cell firing in response to the second stimulus if it had fired in response to the first stimulus. Entrainment measured the proportion of suprathreshold responses out of the total number of stimuli. For measurements of both refractory period and entrainment, the responses to three presentations of a train were averaged at each frequency reported. Successful propagation was defined as an action potential at the soma that also arrived at the axonal recording site. Propagation efficacy was determined by at least 30 events (three trials of 10 stimuli) for each cell. To determine the variability in action potential amplitudes, trains of 100 stimuli were delivered at a single intensity (2 or 5 pA) with stimulus frequency varied between 250 and 1000 Hz. Response trains were chosen in which the rates of rise of somatic action potentials were most variable. Then, at the closest stimulus frequency possible, trains were chosen in which somatic action potentials were uniform. The amplitude of axonal responses was measured (start of rise to peak) for all suprathreshold responses during each of these trains. The standard deviation of action potential amplitudes was measured for each train after normalizing mean action potential amplitude. This measure of variance was averaged across two trains per condition. To compare the amount of action potential amplitude variability across

loose-patch recordings, variability during trains with the least uniform somatic action potentials was divided by variability during trains with highly uniform somatic action potentials. This measure, the variance index, minimized the influence of recording-to-recording differences in noise. Means are presented \pm s.e.m. and compared using either a paired or unpaired Student's *t* test or a one-way ANOVA.

Results

To examine the action potential signalling capabilities of the MSO, whole-cell current-clamp recordings were made from MSO principal neurons in slices taken from gerbils at P17–18. In these recordings, repetitive synaptic stimulation of either ipsilateral or contralateral excitatory afferents could trigger action potential trains at frequencies up to or exceeding 500 Hz (Fig. 1A). These somatic action potentials were small and narrow (rarely exceeding 0 mV), and highly variable across individual responses. Action potential amplitude varied linearly with the rise time of the underlying EPSP. In the single synaptic responses shown in Fig. 1B and C, the amplitude of the action potential increased by \sim 5-fold as the rise time of the EPSP decreased from 0.40 ms near threshold to 0.09 ms. In these experiments, linear correlation coefficients always exceeded 0.63 (mean $r = 0.83 \pm 0.01$, $n = 12$). The dependence of action potential amplitude on EPSP rise time probably reflects substantial shifts in the ratio of sodium to potassium currents underlying the action potential.

To examine whether somatic action potentials and intrinsic membrane properties varied across the tonotopic axis of the MSO, we performed somatic current-clamp recordings from 30 principal cells spanning different tonotopic regions within the MSO of seven individual slices ($n = 2$ –6 cells per slice). Figure 2A shows an example

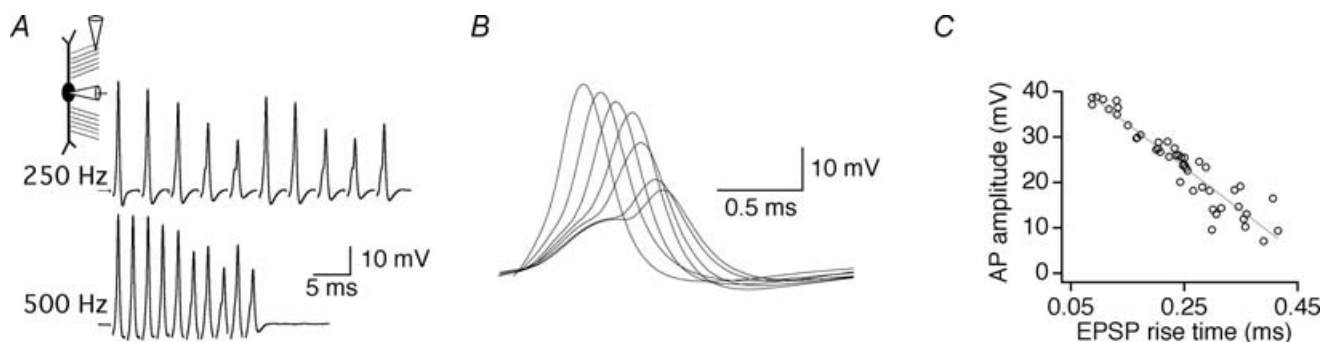


Figure 1. Action potentials are graded at the soma of MSO principal neurons

A, responses to trains of 10 synaptic stimuli show graded somatic action potentials (resting potential, -61 mV; medial stimulation in the presence of $1 \mu\text{M}$ strychnine). B and C, in the same neuron, graded somatic action potentials were evoked by single synaptic shocks. Selected traces are superimposed in B. The amplitudes of 46 action potentials including those in B are plotted in C to show that action potential amplitude correlates linearly ($r^2 = 0.85$) with the rise time of the underlying EPSP.

of six biocytin-filled principal neurons recorded along the dorso-ventral, notopic axis of the MSO (Guinan *et al.* 1972). As shown in Fig. 2B, membrane time constants in this and other slices ranged between 0.28 and 0.56 ms, but did not vary systematically along the dorso-ventral axis within a single slice. When the dorso-ventral axis was subdivided into low-, medium- and high-frequency regions, neither membrane time constants nor peak input resistances varied significantly between these regions (Fig. 2C). Similarly, neither the current threshold nor amplitude of action potentials varied between tonotopic regions (Fig. 2D). At currents well above threshold, action potential amplitudes also showed no tonotopic differences (data not shown). Because of the non-planar nature of their trajectories, MSO axons can be cut at varying lengths during slicing. Each axon was measured to ensure insufficient axonal length did not obscure tonotopic differences in action potential properties. Most of these neurons had axons 100 μm to > 1 mm in length ($n = 18$).

A few neurons with 50–100 μm ($n = 4$) or < 50 μm ($n = 6$) long axons had action potential properties that did not differ systematically from tonotopically similar neurons with longer axons and thus were included. Together these data show that in the MSO, intrinsic membrane properties do not vary along the tonotopic axis and all principal neurons exhibit small, graded action potentials.

Small action potentials at the somas of MSO neurons suggest action potentials also may not propagate efficiently in the dendrites. Propagation of the somatic action potential into the dendrites ('backpropagation') would shape ongoing synaptic integration, and could also influence the induction of synaptic plasticity. To measure the attenuation of backpropagating action potentials, we made dual somatic and dendritic current-clamp recordings and examined action potential amplitude in the soma and dendrites elicited with just supra-threshold current pulses. MSO principal neurons

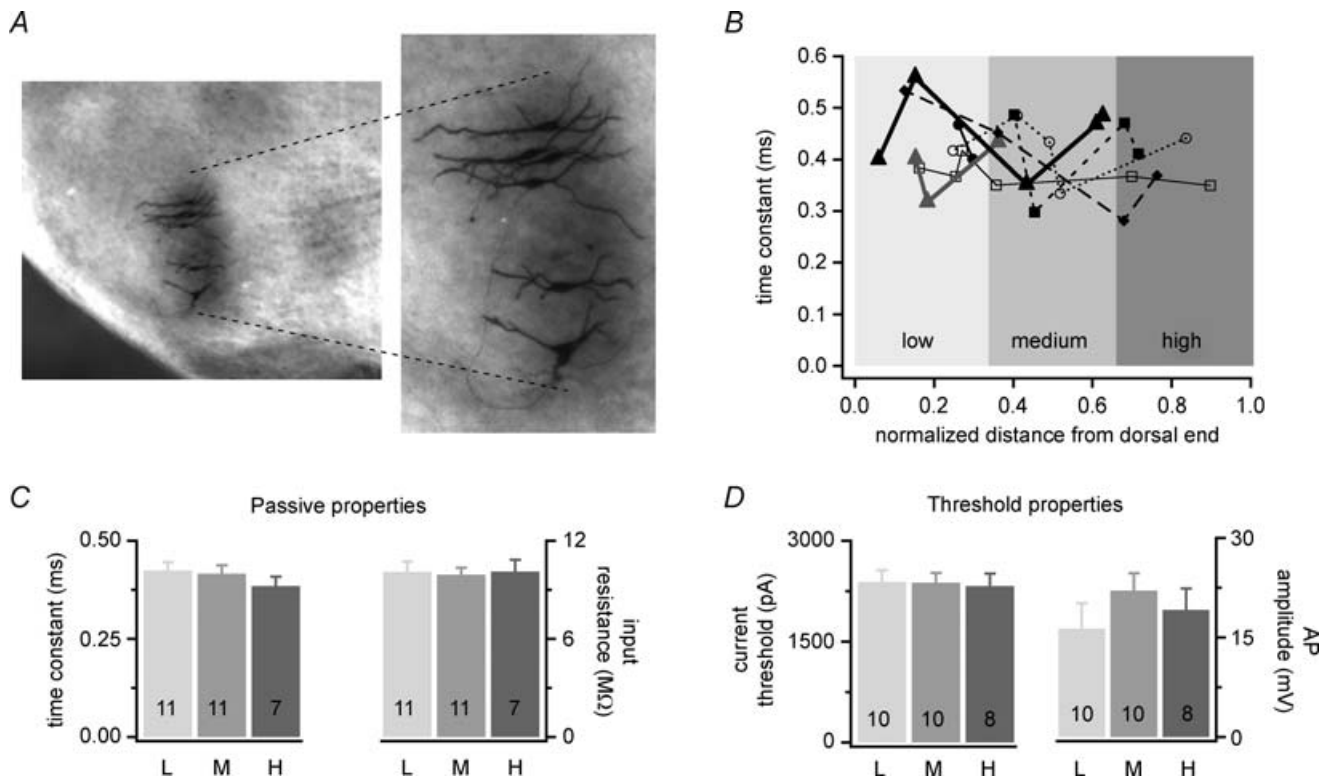


Figure 2. Passive membrane properties and action potential characteristics do not differ along the tonotopic axis of the MSO

A, the dorsal–ventral boundaries of the MSO were visualized with oblique lighting in a coronal brainstem slice (362 μm between the dashed lines). Photomicrographs show six biocytin-labelled MSO principal neurons. Slice oriented with the ventral boundary at the bottom. B, the properties of two to six MSO principal neurons were recorded in each of seven slices. Plotting the properties of neurons within a single MSO as a series (each represented by a unique symbol) shows that the membrane time constants of principal neurons do not vary systematically along the normalized length of the dorsal–ventral axis. The shaded regions represent each third of the MSO estimating the low-, medium- and high-frequency regions. C and D, passive membrane properties and action potential properties at threshold do not vary significantly for neurons in the low- (L), medium- (M) and high-frequency (H) regions. Bar labels display the number of neurons represented in each group.

always fired a single action potential at the onset of the depolarization (Fig. 3A). In all cases, the peaks of the action potentials were detected at the soma prior to the dendrites, with the somato-dendritic delay being proportional to the recording distance (Fig. 3A and B). The conduction velocity of the backpropagating action potential in the dendrites was estimated from the slope of the relative action potential timing *versus* distance plot, and was 1.0 m s^{-1} . The detection of the action potential at the soma prior to the dendrite rules out the possibility that action potentials were dendritically initiated and confirms that action potentials were generated near the soma, presumably in the axon. Consistent with this interpretation, the amplitude of action potentials recorded at the dendrite relative to the soma showed strong attenuation with distance along the dendrite, and could be fitted well with a single exponential (length constant, $76 \mu\text{m}$; Fig. 3C). These measurements underestimate the attenuation of backpropagating action potentials during synaptic activity, which achieves a larger subthreshold dendritic depolarization than somatic current injection.

When action potentials were triggered with synaptic stimuli that depolarized the recorded dendrite, the backpropagating action potential was 85–98% attenuated in amplitude (measured in the distal dendrites between 75 and $120 \mu\text{m}$ from the soma, $n = 5$; Fig. 3D).

Low voltage-activated potassium channels mediated by Kv1 subunits are known to contribute strongly both to the low-input resistance of MSO principal neurons as well as the small amplitude of somatic action potentials. To understand whether these channels also restrict propagation in the dendrites, we examined the effects of α -dendrotoxin (α -DTX), a blocker of Kv1 channel subunits, on the attenuation of backpropagating action potentials in the distal half of the dendritic arbor. In dual recordings from the soma and dendrites between 65 and $90 \mu\text{m}$ away, just-suprathreshold action potential amplitudes at the soma varied widely across cells, ranging from 12 to 38 mV. However, the relative attenuation of the action potential in the dendrites was more consistent: the ratio of dendritic to somatic action potential amplitude ranged from 0.31 to 0.41 (69%–59% attenuation, respectively). In the

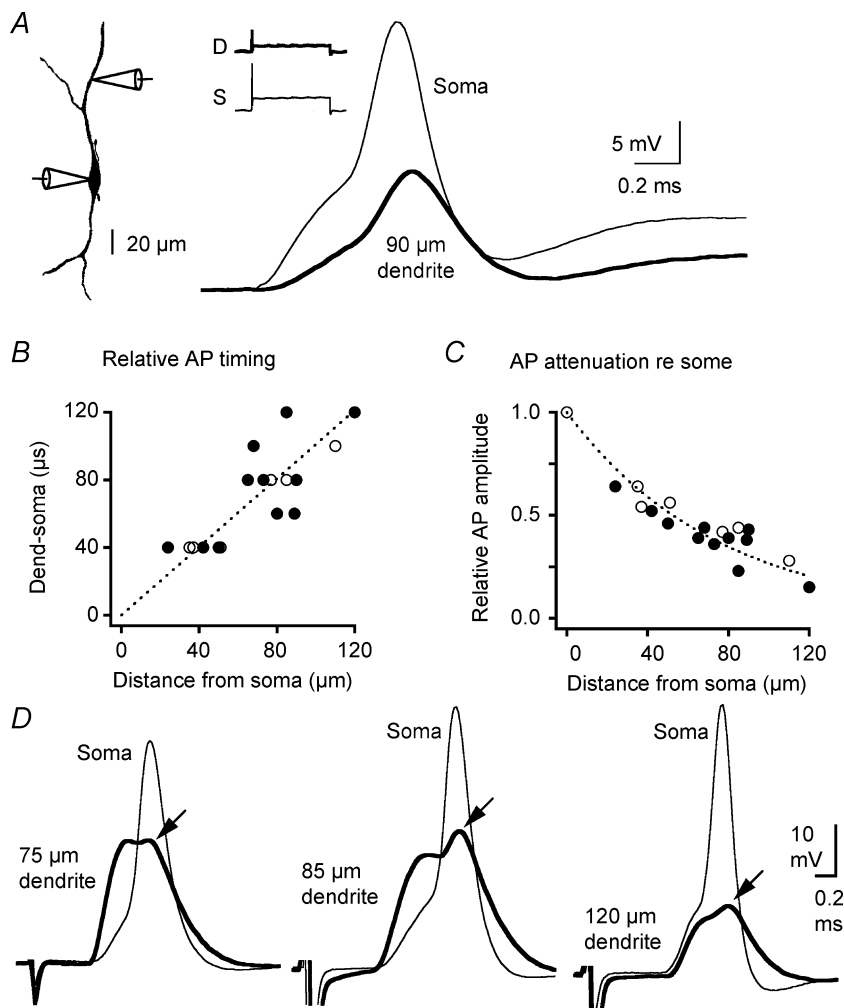


Figure 3. Action potentials heavily attenuate as they backpropagate into the dendrites from the soma

A, Left camera lucida drawing of a biocytin-filled cell shows the location of recording sites in a dual somatic and dendritic current-clamp configuration (resting potential, -62 mV). Right action potential evoked by a 100 ms current pulse (2300 pA) at the soma. Inset shows full-length responses at both recording sites. Somatic and dendritic traces expanded for detail show the action potential arrived first at the soma, and was delayed and attenuated $90 \mu\text{m}$ out on the dendrite. **B**, the timing of the action potential peak at the dendritic recording site increases with distance of the recording site from the soma. \circ , recordings from medial dendrites; \bullet , recordings from lateral dendrites. Linear fit = 1.0 ms^{-1} . **C**, action potentials attenuate strongly as a function of distance along the dendrite. Attenuation expressed as the amplitude of the action potential in the dendrite divided by the amplitude of the action potential at the soma. Symbols as in **B**. Exponential fit; length constant, $76 \mu\text{m}$. **D**, somatic and dendritic traces show responses to suprathreshold synaptic stimulation (resting potential, -62 to -63 mV). In all cases, action potentials appear highly attenuated at the dendritic recording site (arrows). In the rightmost pair of traces, the larger depolarization at the somatic than the dendritic recording site indicates that the majority of inputs were closer to the recording electrode at the soma.

presence of 100 nM α -DTX, action potential amplitude increased by $76 \pm 34\%$ at the soma and $196 \pm 87\%$ in the dendrites, and the attenuation of backpropagating action potentials was reduced from a mean of 53% to 40% ($n = 5$; Fig. 4A and B). The reduction in the rate of rise of subthreshold membrane depolarization is apparent upon the application of toxin, reflecting a substantial increase in input resistance (e.g. Fig. 4A). α -DTX also strongly affected the afterhyperpolarization of the action potential, decreasing its magnitude in the soma and dendrites from -9.8 ± 4.4 and -5.7 ± 2.6 mV, respectively, to -1.0 ± 0.5 and 0.8 ± 0.4 mV, respectively. These results indicate that action potential propagation in the dendrites is shaped in part by low voltage-activated potassium channels. However, the fact that backpropagating action potentials remain unconventionally small even in the presence of α -DTX, indicates that potassium channel activation is

not the only significant factor that limits action potential invasion of the soma and dendrites.

Upon initiation, the attenuation and delayed arrival of the action potential in the dendrite is inconsistent with the interpretation that small somatic action potentials represent remotely initiated spikes in the dendrites. However, graded somatic action potentials could represent remotely initiated spikes in the axon or more proximal axonal initiation with strong and variable attenuation during propagation of spikes to the soma. Also, it is possible that at least some of these small spikes do not represent all-or-none action potential output in the axon, but rather a local semi-regenerative event confined to the soma and/or axon initial segment. To evaluate the efficacy of axonal action potential propagation, we made simultaneous somatic whole-cell recordings and axonal loose-patch recordings from identified MSO principal

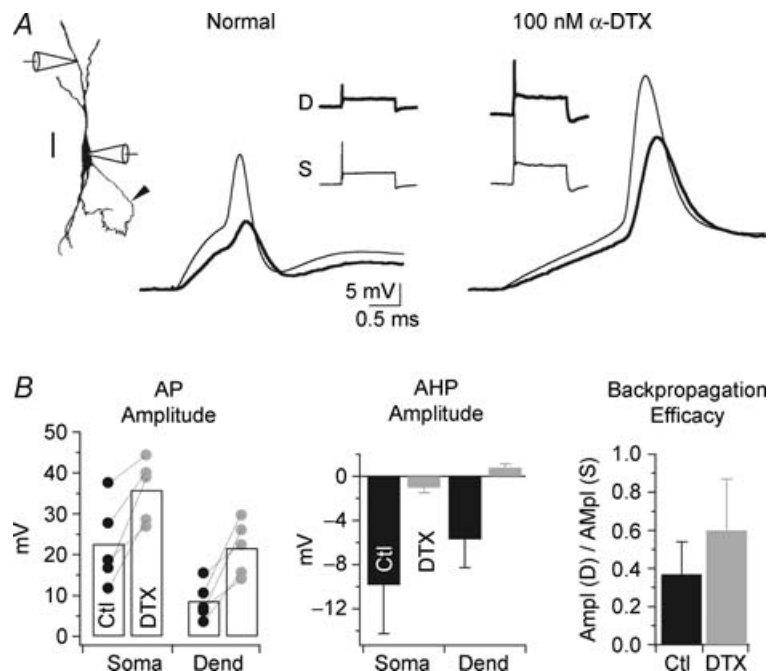


Figure 4. Kv1-containing potassium channels control dendritic attenuation of backpropagating action potentials

A, backpropagating action potentials were initiated with somatic current injection in normal artificial cerebrospinal fluid (ACSF) and in the presence of 100 nM α -dendrotoxin (α -DTX), a blocker of Kv1 potassium channel subunits. Left, a camera lucida reconstruction of the biocytin-labelled cell shows the recording sites at the soma and lateral dendrite, 82 μ m away. The axon (arrowhead) emanated directly from the soma. Scale bar, 20 μ m. Right, expanded view of the backpropagating action potential recorded at the soma (light traces) and the dendrite (dark traces). Insets show the transient firing response of the cell during the 100 ms time course of the current step in both normal ACSF and the presence of α -DTX. Current amplitude: ACSF, 1.6 nA; α -DTX, 0.4 nA. Resting potential: ACSF, -69 mV; α -DTX, -67 mV. B, action potential parameters are shaped by Kv1-containing potassium channels. Left, action potential amplitudes consistently increased in the presence of α -DTX both in the soma and 65–90 μ m away in the dendrites ($n = 5$). Middle, in the same neurons, the application of α -DTX strongly reduced the action potential afterhyperpolarization in both the soma and dendrites. The amplitude of the afterhyperpolarization was measured with respect to the action potential inflection. Right, α -DTX facilitated the propagation of action potentials from the somatic to the dendritic recording site. The degree of backpropagation measured by the dendritic action potential amplitude was normalized to the somatic action potential amplitude.

neurons. When such recordings were made from adjacent locations on the soma, extracellularly recorded action potential voltages were proportional to both the rate of rise and amplitude of the action potential (Fig. 5A), confirming that extracellular recordings are able to detect differences in action potential height and shape. Although the axons of MSO principal neurons are heavily myelinated, axonal loose-patch recordings reliably detected action potentials, even when they appeared small at the soma (Fig. 5B). Furthermore, action potential signals in the axon exhibited the same current thresholds as somatic action potentials (data not shown).

To further explore the relationship between somatic and axonal action potential signals, whole-cell somatic recordings were paired with loose-patch axonal recordings 100–475 μm from the soma. High-frequency trains of brief suprathreshold depolarizations were delivered through the somatic pipette (0.5 ms step, 2–5 nA, 250–1000 Hz, 100 stimuli). Whereas strong current pulses delivered at ~ 500 Hz or less triggered action potentials of uniform amplitude and rate of rise at the soma, higher frequency stimuli closer to the current threshold of a cell triggered action potentials that varied widely in shape during the course of a single train. Regardless of their amplitude and rate of rise at the soma, action potentials were reliably

detected in the axon and did not decline in amplitude even at the highest frequencies (Fig. 6A). When trains from the same recording were divided into groups with either highly variable or uniform somatic action potentials (fixed current, varying frequency), the variance in the amplitudes of the corresponding axonal action potential signals was statistically indistinguishable (paired *t* test $P = 0.24$, $n = 6$; Fig. 6A and B). These results are consistent with the interpretation that action potential signalling in the axon of MSO principal neurons is all-or-none, and independent of the amplitude and rate of rise of the local action potential at the soma. Such a scenario would suggest that action potentials are initiated in the axon and attenuate while propagating through the intervening initial segment to the soma.

Despite differences in somatic and axonal action potential amplitudes, results from paired somatic and axonal recordings are consistent with a proximal zone of action potential initiation (Fig. 7A and B). The traces in Fig. 7A show that for highly graded somatic action potentials, the corresponding axonal signals within recordings were similar in amplitude at sites $> 25 \mu\text{m}$ from the soma. In order to compare the variance of axonal signal amplitudes across recordings exhibiting different levels of noise, the variance in axonal signal

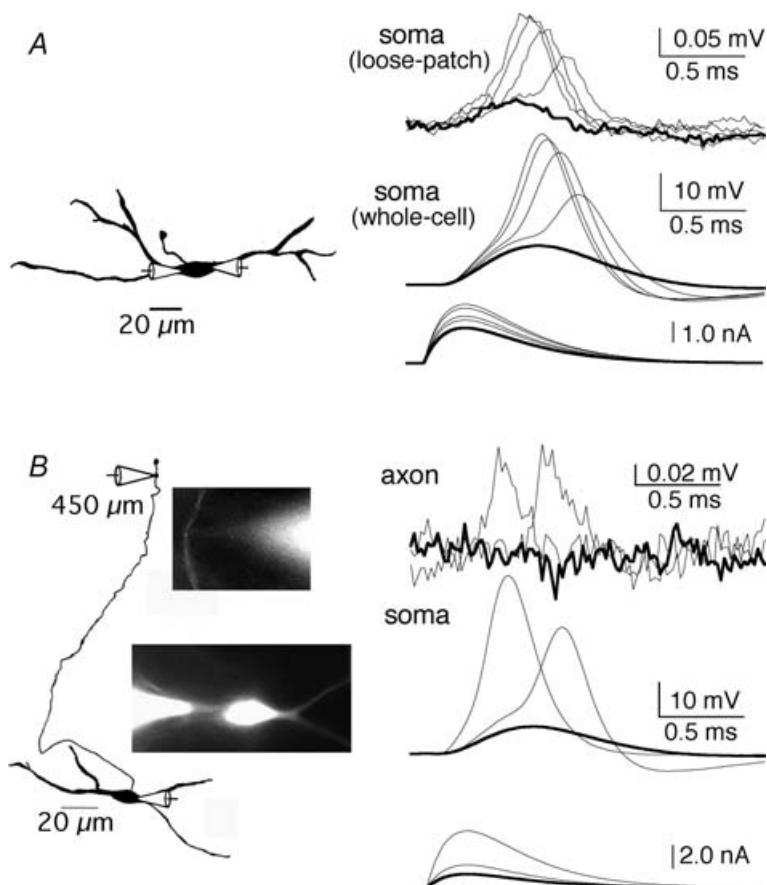


Figure 5. Loose-patch recordings report action potential amplitude and rate of rise

A, camera lucida drawing shows the placement of a loose-patch current-clamp recording pipette and a whole-cell current-clamp recording pipette at the soma of an MSO neuron. Superimposed responses (upper and middle traces) to selected simulated synaptic currents injected at the soma (lower traces). Suprathreshold response amplitudes scale with increasing current amplitudes under both recording conditions (resting potential, -65 mV). Subthreshold traces indicated by thick lines. *B*, camera lucida drawing and fluorescent images taken during the recording show a dual whole-cell somatic recording site and loose-patch axonal recording site $450 \mu\text{m}$ from the soma. Superimposed responses (upper and middle traces) to somatically injected PSC-like waveforms (lower traces). Although suprathreshold responses are graded at the soma, action potential signalling is not graded in the axon. Resting potential, -65 mV. Subthreshold traces indicated by thick lines.

amplitudes during trains of graded somatic spikes was normalized with respect to axonal signal amplitudes arising from uniform somatic spikes in the same recording. Both uniform and non-uniform action potentials were generated with identical current pulses, but at different frequencies. Data were grouped by distance of the axonal recording site from the soma (soma, $n = 5$; 25–50 μm , $n = 5$; 50–100 μm , $n = 3$; > 100 μm , $n = 6$) and show that the normalized variance in axonal signal amplitude was similar for all distances starting 25–50 μm from the soma (one-way ANOVA $P = 0.43$; Fig. 7A and B). To determine the relationship between this proximal axonal region and the initial segment, we combined single-cell biocytin labelling with immunocytochemical staining for myelin basic protein (see Methods; Fig. 7C). Myelin basic protein labelling was detected within 17–28 μm of the soma (mean, $21 \pm 0.71 \mu\text{m}$, $n = 6$). Together, these results suggest that all-or-none action

potentials are initiated proximally in the axon, near the start of myelination, and undergo unusually strong attenuation during backpropagation into the soma and dendrites.

The shape and amplitude of axonal action potential signals remained uniform during high-frequency trains at all recording distances tested. To better characterize the reliability of high-frequency firing and signal propagation in MSO principal neurons, a paired-pulse protocol was delivered during dual somatic whole-cell and axonal loose-patch recordings > 100 μm from the soma. With weak suprathreshold stimuli (2 nA, 0.5 ms step duration), action potentials were detected at both recording sites for interpulse intervals as low as 1 ms ($n = 5$; Fig. 8B). However, with larger stimuli more than twice the current threshold (5 nA), MSO principal cells could respond to the second test pulse at intervals as low as 0.7 ms (Fig. 8A and B). Thus, MSO neurons have a submillisecond

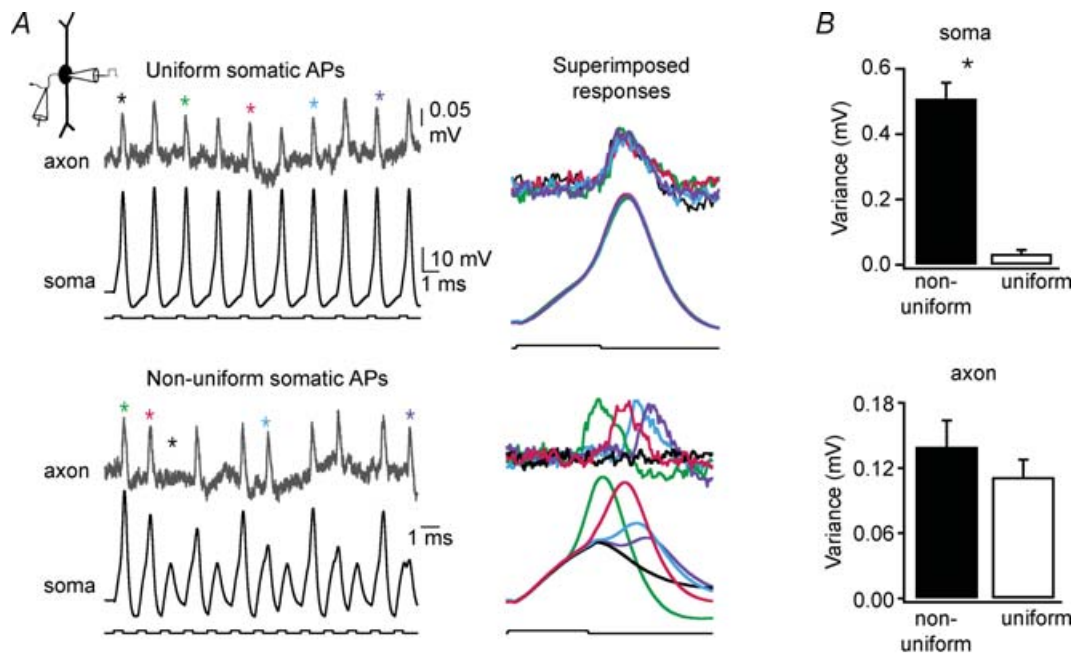


Figure 6. Action potentials are 'all-or-none' in the axon, even during long trains or when action potentials are graded at the soma

A, adjusting the frequency of somatically injected current pulses (100 stimuli, 2 nA) altered the level of uniformity in the rate of rise and amplitude of somatic action potentials. In this case, high uniformity occurred at 500 Hz (upper panel) while minimal uniformity occurred at 750 Hz (lower panel). In each panel, traces on the left show somatic and axonal (450 μm from the soma) responses to the first 10–13 stimuli in each train (resting potential, -60 mV). Responses marked with asterisks are superimposed on the right. All responses on the right are suprathreshold except the black trace in the lower panel. For trains with uniform somatic action potentials, somatic and axonal action potentials occurred in response to each pulse and remained constant in rate of rise and amplitude for the duration of the train. When action potential amplitudes and rates of rise varied at the soma, signals were constant in amplitude in the axon and occurred even when somatic action potentials were $< 5 \text{ mV}$. B, as in A, the frequency of stimulus trains (100 stimuli, 2 nA) was adjusted to achieve either the most uniform or non-uniform rates of rise for somatic action potentials (250–500 Hz and 500–1000 Hz, respectively). Axonal recording sites were > 100 μm from the soma. As expected, the variance (standard deviation) in the rates of rise for somatic action potentials differs substantially between these groups (upper histogram, paired t test $*P < 0.0005$, $n = 6$). However, the variance in the amplitudes for axonal action potential signals did not differ between these groups (lower histogram, paired t test $P = 0.24$, $n = 6$). Standard deviations were obtained from normalized means.

absolute refractory period for action potential initiation and propagation in the axon.

Short refractory periods allow MSO neurons to entrain to high-frequency stimulation. Perfect entrainment occurred in response to trains of 10 somatically injected current pulses at frequencies up to 600–1000 Hz, depending upon the strength of stimulation ($n = 5$; Fig. 9A and B). Even at 1400 Hz, neurons generated precisely timed action potential output, despite the fact that some stimulus cycles were skipped (Fig. 9A). Although graded, somatic action potentials reliably reflected action potential initiation and propagation in the axon (Fig. 9C).

Discussion

Principal neurons of the MSO detect the temporal coincidence of binaural inputs, which fire at high

frequencies, and convey this information to higher auditory centres through their rate of action potential firing. The manner in which synaptic excitation is transformed into action potential output is thus a key process regulating ITD encoding in the MSO. Our previous work has shown that MSO neurons exhibit graded action potentials that average < 10 mV in amplitude at the soma after the fourth postnatal week (Scott *et al.* 2005). In the current study, we have shown that these graded action potentials undergo strong attenuation in the dendrites particularly during synaptic excitation. Despite their unconventional characteristics at the soma, action potentials are initiated in or near the axon initial segment, and are associated with remarkably secure axonal signalling even at frequencies exceeding 1 kHz. The strong electrical segregation of action potentials from the somato-dendritic compartment of the cell curtails

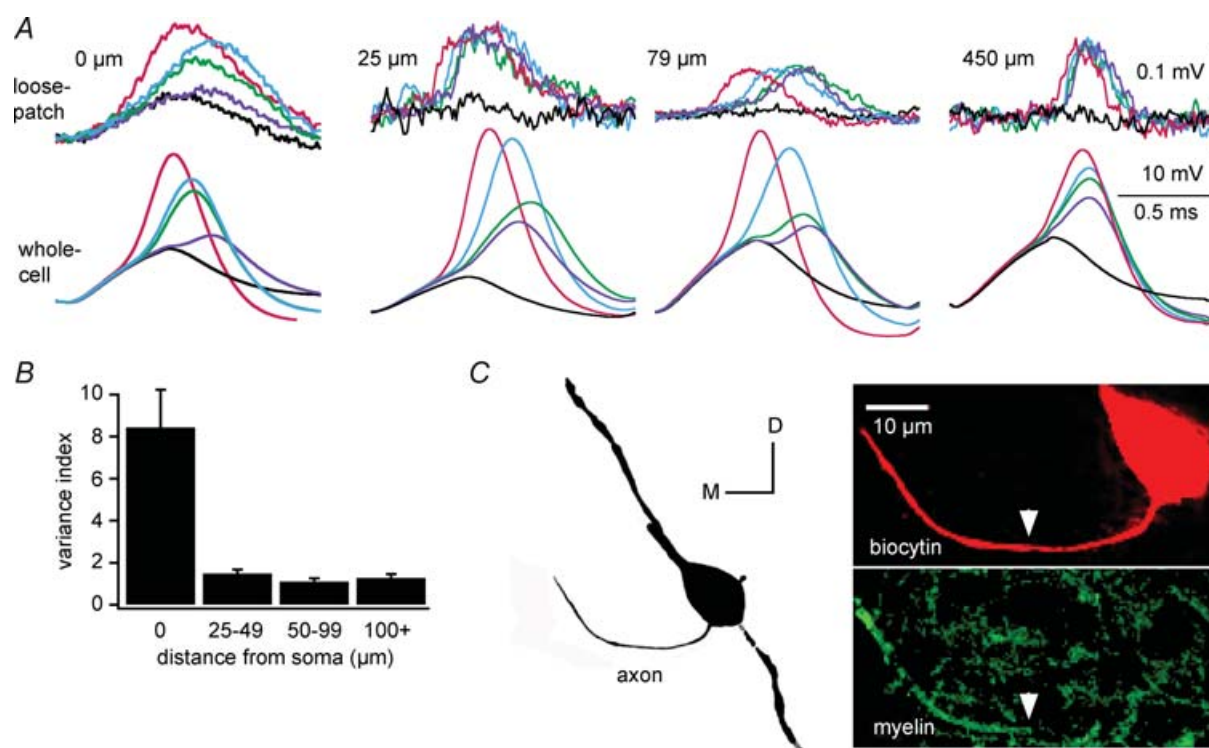


Figure 7. Action potentials are 'all-or-none' beyond the initial segment

A, selected, superimposed loose-patch and whole-cell responses to somatically injected current pulses delivered during 100-stimulus trains (resting potential, -59 to -65 mV). Whole-cell recordings at the soma. Loose-patch recordings 0, 25, 79 and $450 \mu\text{m}$ from the soma. Corresponding responses are colour-matched. Subthreshold responses are black. Action potential signals were graded at the soma and all-or-none at all axonal locations. B, the histogram shows the variability in the amplitude of action potentials during loose-patch recordings grouped by distance from the soma ($n = 5, 5, 3$ and 6 , respectively). The variance in action potential amplitudes was significantly larger at the soma than the axon (unpaired t test $P < 5 \times 10^{-6}$). At recording sites $> 25 \mu\text{m}$ from the soma, the variance of action potential amplitudes did not differ significantly (one-way ANOVA $P = 0.43$). The variance index is the ratio of the standard deviation during trains with graded somatic action potentials to the standard deviation during trains with uniform somatic action potentials. Standard deviations were obtained from normalized means. C, left, partial camera lucida reconstruction of a biocytin-filled neuron in a slice that was sectioned at $30 \mu\text{m}$ for immunohistochemistry. Right, a composite image including 97 optical slices (slice thickness, $0.122 \mu\text{m}$) shows staining for biocytin (red) and myelin basic protein (green) in the same neuron. Myelination of the axon begins within $24 \mu\text{m}$ of the soma (arrow).

distortions in the timing and amplitude of synaptic activity by action currents, and may be an important mechanism to maintain the precision of binaural comparisons at high frequencies.

Action potential initiation

Our results demonstrate an unusually strict electrical segregation of the soma and dendrites from the axonal initiation zone in MSO principal neurons. Graded action potentials at the soma, which could range from just a few millivolts to tens of millivolts, were tightly associated with uniform action potential output in the axon when detected at distances beyond $\sim 25 \mu\text{m}$. The region of the axon proximal to this location corresponded to the unmyelinated initial segment, as revealed by immunocytochemical labelling for myelin basic protein. These results are consistent with data from both classical studies and more recent examinations indicating that the site of action potential initiation is in the vicinity of the distal initial segment or first heminode of the axon (Coombs *et al.* 1957; Palmer & Stuart, 2006; Khaliq & Raman, 2006; Meeks *et al.* 2007). One significant difference between MSO principal neurons and these other neuron types, however, is the extraordinary security and uniformity of axonal signalling at frequencies up to and exceeding 1 kHz. These results indicate that the axon of MSO principal neurons is specialized for high-frequency signalling.

One specialization supporting the capacity to follow high-frequency stimulation is a high resting conductance in MSO principal neurons, which in turn enables fast membrane voltage changes. The high axonal firing frequencies (up to ~ 1 kHz) observed in the present study would suggest that the axon possesses unusually fast membrane properties as well. In our previous report we showed that the membrane time constants of principal MSO neurons undergo a developmental decrease throughout the ages used in the current study (Scott *et al.* 2005). Thus the frequency-following capabilities reported here may underestimate the capacity of mature neurons. The properties and density of sodium channels in the axon also determines the frequency limits of axonal firing. In neurons of the medial nucleus of the trapezoid body as well as their calyceal inputs, rapid channel kinetics and fast recovery from inactivation ensures brief action potentials and short refractory periods. These properties in turn enable reliable firing at frequencies of hundreds of hertz (Leao *et al.* 2005). In MSO principal neurons, while the density of sodium channels in the initial segment is clearly sufficient to initiate action potentials securely at high frequency, it is not known whether such firing requires a density of sodium channels greatly exceeding that necessary for a single action potential, as has been found in hippocampal neurons (Madeja, 2000).

The question arises as to how action potentials can be so severely restricted from the soma of MSO

neurons, given the short distances ($< 30 \mu\text{m}$) that the action potential travels in the initial segment. The diminutive, graded nature of somatic action potentials demonstrates a highly unfavourable ratio of inward sodium currents to outward potassium currents, preventing strong regenerative excitation. Previous studies have demonstrated a high sensitivity of action potentials in the soma of MSO neurons to blockade of low voltage-activated potassium channels with different fractions of dendrotoxins (Svirskis *et al.* 2002, 2004; Scott *et al.* 2005), indicating that Kv1-containing potassium channels tightly control action potential invasion of the soma from the axon. The soma and large-calibre dendrites themselves may further attenuate backpropagating action potentials by providing a substantial capacitive load, reducing the impact of depolarizing currents. The distribution and subunit composition of voltage-gated sodium channels in MSO principal cells is not currently known.

Tonotopic uniformity

We did not observe systematic differences in action potential characteristics or passive membrane properties as a function of location along the tonotopic axis of the MSO. When we recorded up to six neurons across

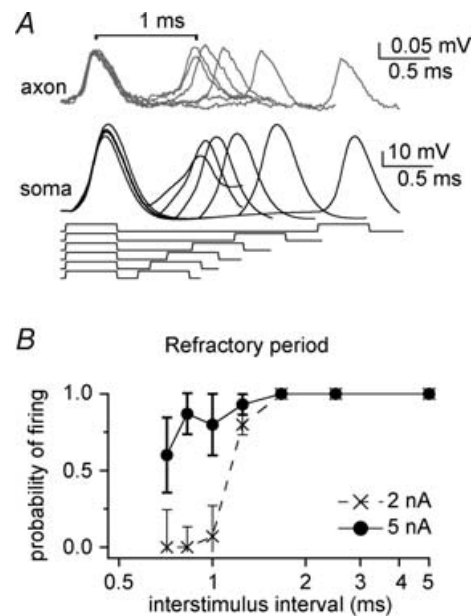


Figure 8. Measurements of action potential refractory period

A, dual whole-cell somatic and loose-patch axonal recording shows the responses to two somatically injected square current pulses (0.5 ms, 5 nA; responses superimposed). Axonal recording at $104 \mu\text{m}$; resting potential, -58 mV. Action potentials are evoked by each stimulus presented at interstimulus intervals from 5 to 0.7 ms.

B, semi-logarithmic plot of the group means for five cells shows that the probability of firing in response to each of two stimuli (2 or 5 nA) remains high until interstimulus intervals approach 1 ms. Axonal recordings were 104 to $474 \mu\text{m}$ from the soma.

the tonotopic axis of the MSO in single slices, we noted differences in membrane time constants between neurons on the scale of only a few hundred microseconds. In addition, the extremes of the range of intrinsic properties and action potential amplitudes could be observed in neighbouring neurons. These findings stand in contrast to studies of the avian nucleus laminaris (NL), the analogue to MSO in birds. In NL, membrane time constants, EPSP half-widths, and action potential amplitudes vary according to tonotopic region, presumably reflecting regional differences in the expression of both sodium and potassium channel subunits (Parameshwaran *et al.* 2001; Kuba *et al.* 2005, 2006). The fact that membrane properties and action potential characteristics did not vary tonotopically in the MSO may not represent a general difference in the time-coding auditory nuclei of birds and mammals. In young rodents, neurons of the lateral superior olive and medial nucleus of the trapezoid body (MNTB) display differences in firing properties as well as differences in the expression of potassium and/or HCN channel subunits as a function of tonotopic location (Barnes-Davies *et al.* 2004; Song *et al.* 2005; Leao *et al.* 2006).

Action potential propagation in the dendrites

We found that action potentials in MSO neurons undergo strong attenuation as they propagate from the soma into the distal dendrites, failing to amplify and only modestly prolonging underlying synaptic potentials. Additionally, depolarization of the dendrites as distal as 120 μm , either through synaptic stimulation or current injection, failed to elicit dendritic electrogenesis. These findings contrast sharply with the more common scenario in hippocampal, cortical and mitral neurons, in which regenerative, but decreased propagation of the action potential is sustained through the activation of voltage-gated sodium channels present in the dendrites (Stuart & Sakmann, 1994; Spruston *et al.* 1995; Magee & Johnston, 1995; Bischofberger & Jonas, 1997). These channels can also mediate local, fast sodium spikes in response to dendritic excitation independent of action potential initiation in the axon (Stuart *et al.* 1997; Gullidge *et al.* 2005; Holthoff *et al.* 2006). In Purkinje neurons of the cerebellum, propagation of sodium-dependent action potentials in the dendrites shows strong attenuation, as in MSO principal neurons (Llinás & Sugimori, 1980). The strong attenuation is

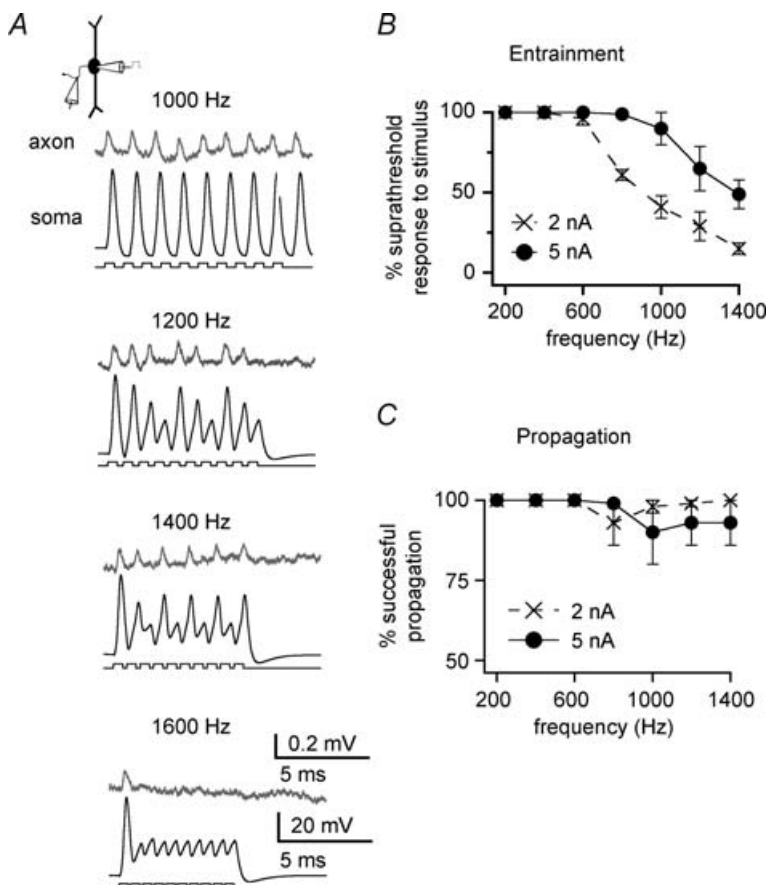


Figure 9. Action potentials initiated at high frequencies propagate securely in the axon

A, dual whole-cell somatic and loose-patch axonal recording shows perfect entrainment to 10 somatically injected current pulses (0.05 ms, 5 nA) at frequencies up to 1400 Hz (axonal recording at 104 μm ; resting potential, -58 mV). Entrainment ceases at 1600 Hz. **B**, plot displays mean entrainment for the stimulus protocol in **A** across five neurons (axonal recordings at 104 to 474 μm ; 2 or 5 nA current pulses). **C**, for the same stimulus protocol and cells as **B**, plot shows the percentage of action potentials recorded at the soma that successfully propagated to the axonal recording site 104 to 474 μm from the soma. Propagation fidelity did not drop off significantly at frequencies up to 1400 Hz.

associated with a decline in sodium channel density in the dendrites (Stuart & Häusser, 1994). Our results do not preclude the presence of voltage-gated sodium or calcium channels in MSO dendrites, but under the conditions that we have examined in the slice, inward sodium currents fail to sustain highly regenerative propagation in the dendrites.

Low voltage-activated potassium channels contribute to the attenuation of backpropagating action potentials in the dendrites of MSO principal neurons. When backpropagating action potentials were recorded during blockade of low voltage-activated potassium channels with α -DTX, the attenuation of these action potentials was reduced from 53% to 40%. There are two primary mechanisms underlying these effects. First, because low voltage-activated potassium channels are partially activated at the resting potential, their blockade increases the input resistance of the cell, making the cell more electrotonically compact and increasing the passive spread of voltage changes along the dendrites. Second, reduction of action potential repolarization by α -DTX, reflected in the near-elimination of the afterhyperpolarization, increased action potential amplitude in both the soma and dendrites. Despite these effects, backpropagating action potentials remained unconventionally small even in the presence of α -DTX, indicating that potassium conductances are not wholly responsible for the weak regenerative properties of MSO principal neuron dendrites.

Functional implications

Action potential initiation is unusually reliable in MSO principal neurons, with axonal and somatic action potentials tightly associated at stimulus frequencies exceeding 1 kHz. Only when the soma was driven repetitively with long trains at 1 kHz were axonal or somatic action potentials observed to occur in isolation from one another in a few MSO principal neurons. The strong association of somatic and axonal signals probably reflects the proximity of the soma to action potential electrogenesis in the axon/initial segment. However, initiation of action potentials in this proximal axonal zone is not translated into large depolarizations at the soma, where weak action currents provide little or no local amplification.

Are limited action currents, particularly in the cell body and dendrites, a necessary feature for high-frequency firing? Pacemaker neurons in the weakly electric fish fire at rates > 1 kHz and have small, ~30 mV somatic action potentials (Dye, 1991). However, fast-spiking cortical neurons have large amplitude somatic action potentials and, with strong, prolonged depolarization *in vitro*, will elicit somatic spikes at ~500–600 Hz (Connors & Gutnick, 1990). One caveat is that long-lasting depolarization of the soma can broaden axonal action potentials, and in turn

restrict high-frequency axonal firing (Shu *et al.* 2006). Even with lower maximal spike frequencies (30–300 Hz), under similar conditions cerebellar Purkinje and CA3 pyramidal neurons experience axonal propagation failures (Meeks *et al.* 2005; Khaliq & Raman, 2005; Monsivais *et al.* 2005).

The difference in action potential properties between higher order neurons and brainstem auditory neurons such as those in the MSO may have as much to do with the nature of synaptic integration as the demands for high-frequency firing. Excitatory and inhibitory projections from spherical bushy cells and principal neurons of the MNTB, respectively, show high entrainment and phase locking to both tones and broadband acoustic stimuli. A single MSO neuron collectively receives inputs firing at rates up to ~800 Hz, and instantaneous frequencies can approach ~1.5 kHz (Rose *et al.* 1974; Joris *et al.* 1994; Kopp-Scheinflug *et al.* 2003; Louage *et al.* 2005). Thus in MSO neurons there is a need not only to minimize the temporal window over which each binaural comparison is made, but also to reduce the influence of a given integrative cycle on future cycles. Restriction of action potentials and their strong, non-linear afterhyperpolarizations from the soma and dendrites would be expected to reduce the sensitivity of high-frequency synaptic integration on the recent history of firing of the cell.

References

- Agmon-Snir H, Carr CE & Rinzel J (1998). The role of dendrites in auditory coincidence detection. *Nature* **393**, 268–272.
- Barnes-Davies M, Barker MC, Osmani F & Forsythe ID (2004). Kv1 currents mediate a gradient of principal neuron excitability across the tonotopic axis in the rat lateral superior olive. *Eur J Neurosci* **19**, 325–333.
- Bischofberger J & Jonas P (1997). Action potential propagation into the presynaptic dendrites of rat mitral cells. *J Physiol* **504**, 359–365.
- Brand A, Behrend O, Marquardt T, McAlpine D & Grothe B (2002). Precise inhibition is essential for microsecond interaural time difference coding. *Nature* **417**, 543–547.
- Connors BW & Gutnick MJ (1990). Intrinsic firing patterns of diverse neocortical neurons. *Trends Neurosci* **13**, 99–104.
- Coombs JS, Curtis DR & Eccles JC (1957). The interpretation of spike potentials of motoneurons. *J Physiol* **139**, 198–231.
- Dye J (1991). Ionic and synaptic mechanisms underlying a brainstem oscillator: an *in vitro* study of the pacemaker nucleus of *Apteronotus*. *J Comp Physiol A Neuroethol Sens Neural Behav Physiol* **168**, 521–532.
- Gerstner W, Kempter R, van Hemmen JL & Wagner H (1996). A neuronal learning rule for sub-millisecond temporal coding. *Nature* **383**, 76–81.
- Goldberg JM & Brown P (1969). Response of binaural neurons of dog superior olivary complex to dichotic tonal stimuli: some physiological mechanisms of sound localization. *J Neurophysiol* **32**, 613–636.

- Grothe B (2003). New roles for synaptic inhibition in sound localization. *Nat Rev Neurosci* **4**, 540–550.
- Guinan JJ Jr, Norris BE & Guinan SS (1972). Single auditory units in the superior olivary complex. II. Locations of unit categories and tonotopic organization. *Int J Neurosci* **4**, 147–166.
- Gulledge AT, Kampa BM & Stuart GJ (2005). Synaptic integration in dendritic trees. *J Neurobiol* **64**, 75–90.
- Häusser M, Spruston N & Stuart GJ (2000). Diversity and dynamics of dendritic signaling. *Science* **290**, 739–744.
- Holthoff K, Kovalchuk Y & Konnerth A (2006). Dendritic spikes and activity-dependent synaptic plasticity. *Cell Tissue Res* **326**, 369–377.
- Joris P, Carney LH, Smith PH & Yin TC (1994). Enhancement of neural synchronization in the anteroventral cochlear nucleus. I. Responses to tones at the characteristic frequency. *J Neurophysiol* **71**, 1022–1036.
- Joris P & Yin TC (2007). A matter of time: internal delays in binaural processing. *Trends Neurosci* **30**, 70–78.
- Kapfer C, Seidl AH, Schweizer H & Grothe B (2002). Experience-dependent refinement of inhibitory inputs to auditory coincidence-detector neurons. *Nat Neurosci* **5**, 247–253.
- Khalilq ZM & Raman IM (2005). Axonal propagation of simple and complex spikes in cerebellar Purkinje neurons. *J Neurosci* **25**, 454–463.
- Khalilq ZM & Raman IM (2006). Relative contributions of axonal and somatic Na channels to action potential initiation in cerebellar Purkinje neurons. *J Neurosci* **26**, 1935–1944.
- Kopp-Scheinflug C, Lippe WR, Dörrscheidt GJ & Rübsamen R (2003). The medial nucleus of the trapezoid body in the gerbil is more than a relay: comparison of pre- and postsynaptic activity. *J Assoc Res Otolaryngol* **4**, 1–23.
- Kuba H, Ishii TM & Ohmori H (2006). Axonal site of spike initiation enhances auditory coincidence detection. *Nature* **444**, 1069–1072.
- Kuba H, Yamada R, Fukui I & Ohmori H (2005). Tonotopic specialization of auditory coincidence detection in nucleus laminaris of the chick. *J Neurosci* **25**, 1924–1934.
- Leao R, Kushmerick C, Pinaud R, Renden R, Li G-L, Taschenberger H, Spirou G, Levinson SR & von Gersdorff H (2005). Presynaptic Na⁺ channels: locus, development, and recovery from inactivation at a high-fidelity synapse. *J Neurosci* **25**, 3724–3738.
- Leao R, Sun H, Svahn K, Berntson A, Youssoufian M, Paolini AG, Fyffe RE & Walmsley B (2006). Topographic organization in the auditory brainstem of juvenile mice is disrupted in congenital deafness. *J Physiol* **571**, 563–578.
- Lindsey BG (1975). Fine structure and distribution of axon terminals from the cochlear nucleus on neurons in the medial superior olivary nucleus of the cat. *J Comp Neurol* **160**, 81–103.
- Llinás R & Sugimori M (1980). Electrophysiological properties of in vitro Purkinje cell dendrites in mammalian cerebellar slices. *J Physiol* **305**, 197–213.
- Louage DH, van der Heijden M & Joris PX (2005). Enhanced temporal response properties of anteroventral cochlear nucleus neurons to broadband noise. *J Neurosci* **25**, 1560–1570.
- Madeja M (2000). Do neurons have a reserve of sodium channels for the generation of action potentials? A study on acutely isolated CA1 neurons from the guinea-pig hippocampus. *Eur J Neurosci* **12**, 1–7.
- Magee JC & Johnston D (1995). Characterization of single voltage-gated Na⁺ and Ca²⁺ channels in apical dendrites of rat CA1 pyramidal neurons. *J Physiol* **487**, 67–90.
- Meeks JP, Jiang X & Mennerick S (2005). Action potential fidelity during normal and epileptiform activity in paired soma-axon recordings from rat hippocampus. *J Physiol* **566**, 425–441.
- Meeks JP, Jiang X & Mennerick S (2007). Action potential initiation and propagation in CA3 pyramidal axons. *J Neurophysiol* **97**, 3460–3472.
- Monsivais P, Clark BA, Roth A & Häusser M (2005). Determinants of action potential propagation in cerebellar Purkinje cell axons. *J Neurosci* **25**, 464–472.
- Palmer AR (2004). Reassessing mechanisms of low-frequency sound localisation. *Curr Opin Neurobiol* **14**, 457–460.
- Palmer LM & Stuart GJ (2006). Site of action potential initiation in layer 5 pyramidal neurons. *J Neurosci* **26**, 1854–1863.
- Parameshwaran S, Carr CE & Perney TM (2001). Expression of the Kv3.1 potassium channel in the avian auditory brainstem. *J Neurosci* **21**, 485–494.
- Rose JE, Kitzes LM, Gibson MM & Hind JE (1974). Observations on phase-sensitive neurons of anteroventral cochlear nucleus of the cat: nonlinearity of cochlear output. *J Neurophysiol* **37**, 218–253.
- Scott LL, Mathews PJ & Golding NL (2005). Posthearing developmental refinement of temporal processing in principal neurons of the medial superior olive. *J Neurosci* **25**, 7887–7895.
- Shu Y, Hasenstaub A, Duque A, Yu Y & McCormick DA (2006). Modulation of intracortical synaptic potentials by presynaptic somatic membrane potential. *Nature* **441**, 761–765.
- Smith PH (1995). Structural and functional differences distinguish principal from nonprincipal cells in the guinea pig MSO slice. *J Neurophysiol* **73**, 1653–1667.
- Song P, Yang Y, Barnes-Davies M, Bhattacharjee A, Hamann M, Forsythe ID, Oliver DL & Kaczmarek LK (2005). Acoustic environment determines phosphorylation state of the Kv3.1 potassium channel in auditory neurons. *Nat Neurosci* **8**, 1335–1342.
- Spitzer MW & Semple MN (1995). Neurons sensitive to interaural phase disparity in gerbil superior olive: diverse monaural and temporal response properties. *J Neurophysiol* **73**, 1668–1690.
- Spruston N, Schiller Y, Stuart G & Sakmann B (1995). Activity-dependent action potential invasion and calcium influx into hippocampal CA1 dendrites. *Science* **268**, 297–300.
- Stuart G & Häusser M (1994). Initiation and spread of sodium action potentials in cerebellar Purkinje cells. *Neuron* **13**, 703–712.
- Stuart G & Sakmann B (1994). Active propagation of somatic action potentials into neocortical pyramidal cell dendrites. *Nature* **367**, 69–72.

- Stuart G, Spruston N, Sakmann B & Häusser M (1997). Action potential initiation and backpropagation in neurons of the mammalian CNS. *Trends Neurosci* **20**, 125–131.
- Svirskis G, Kotak V, Sanes DH & Rinzel J (2002). Enhancement of signal-to-noise ratio and phase locking for small inputs by a low-threshold outward current in auditory neurons. *J Neurosci* **22**, 11019–11025.
- Svirskis G, Kotak V, Sanes DH & Rinzel J (2004). Sodium along with low-threshold potassium currents enhance coincidence detection of subthreshold noisy signals in MSO neurons. *J Neurophysiol* **91**, 2465–2473.
- Yin TC & Chan JCK (1990). Interaural time sensitivity in medial superior olive of cat. *J Neurophysiol* **64**, 465–488.
- Zhou Y, Carney LH & Colburn HS (2005). A model for interaural time difference sensitivity in the medial superior olive: interaction of excitatory and inhibitory synaptic inputs, channel dynamics, and cellular morphology. *J Neurosci* **25**, 3046–3058.

Acknowledgements

We would like to thank Sukant Khurana and Paul Mathews for helpful comments regarding the manuscript, as well as Angela Bardo for technical assistance with confocal microscopy. This work was supported by a grant from the National Institute of Deafness and Communication Disorders (RO1-DC006877 to N.L.G.), and a postdoctoral Ruth Kirschstein National Research Service Award (F32-DC007245 to L.L.S.).